Biogeography & Environmental Conditions Shape Phage & Bacteria Interaction Networks Across the Human Microbiome

Geoffrey D Hannigan[1], Melissa B Duhaime[2], Danai Koutra[3], and Patrick D Schloss[1,*]

[1]Department of Microbiology & Immunology, University of Michigan, Ann Arbor, Michigan, 48109

[2]Department of Ecology & Evolutionary Biology, University of Michigan, Ann Arbor, Michigan, 48109

[3]Department of Computer Science, University of Michigan, Ann Arbor, Michigan, 48109

[*]To whom correspondence may be addressed.

Running Title: Network Diversity of the Healthy Human Microbiome

Corresponding Author Information

Patrick D Schloss, PhD

1150 W Medical Center Dr. 1526 MSRB I

Ann Arbor, Michigan 48109

Phone: (734) 647-5801

Email: pschloss@umich.edu

Abstract

Viruses and bacteria are critical components of the human microbiome and play important roles in health and disease. Most previous work has relied on studying microbes and viruses independently, thereby reducing them to two separate communities. Such approaches are unable to capture how these microbial communities interact, such as through processes that maintain community stability or allow phage-host populations to co-evolve. We developed and implemented a network-based analytical approach to describe phage-bacteria network diversity throughout the human body. We accomplished this by building a machine learning algorithm to predict which phages could infect which bacteria in a given microbiome. This algorithm was applied to paired viral and bacterial metagenomic sequence sets from three previously published human cohorts. We organized the predicted interactions into networks that allowed us to evaluate phage-bacteria connectedness across the human body. We found that gut and skin network structures were person-specific and not conserved among cohabitating family members. High-fat diets and obesity appeared to be associated with less connected networks. Network structure differed between skin sites, with those exposed to the external environment being less connected and more prone to instability. This study quantified and contrasted the diversity of virome-microbiome networks across the human body and illustrated how environmental factors may influence phage-bacteria interactive dynamics. This work provides a baseline for future studies to better understand system perturbations, such as disease states, through ecological networks.

Importance

The human microbiome, the collection of microbial communities that colonize the human body, is a crucial component to health and disease. Two major components to the human microbiome are the bacterial and viral communities. These communities have primarily been studied separately using metrics of community composition and diversity. These approaches have failed to capture the complex dynamics of interacting bacteria and phage communities, which frequently share genetic information and work together to maintain stable ecosystems. Removal of bacteria or phage can disrupt or even collapse those ecosystems. Relationship-based network approaches allow us to capture this interaction information. Using this network-based approach with three independent human cohorts, we were able to present an initial understanding of how phage-bacteria networks differ throughout the human body, so as to provide a baseline for future studies of how and why microbiome networks differ in disease states.

Introduction

Viruses and bacteria are critical components of the human microbiome and play important roles in health and disease. Bacterial communities have been associated with disease states, including a range of skin conditions (1), acute and chronic wound healing conditions (2, 3), and gastrointestinal diseases, such as inflammatory bowel disease (4, 5), *Clostridium difficile* infections (6) and colorectal cancer (7, 8). Altered human viromes (virus communities consisting primarily of bacteriophages) also have been associated with diseases and perturbations, including inflammatory bowel disease (5, 9), periodontal disease (10), spread of antibiotic resistance (11), and others (12–17). Viruses act in concert with their microbial hosts as a single ecological community (18). Viruses influence their living microbial host communities through processes including lysis, host gene expression modulation (19), influence on evolutionary processes such as horizontal gene transfer (22) or antagonistic co-evolution (26), and alteration of ecosystem processes and elemental stoichiometry (27).

Previous human microbiome work has focused on bacterial and viral communities, but have reduced them to two separate communities by studying them independently (5, 9, 10, 12–17). This approach fails to capture the complex dynamics of interacting bacteria and phage communities, which frequently share genetic information and work together to maintain stable ecosystems. Removal of bacteria or phages can disrupt or even collapse those ecosystems (18, 28–37). Relationship-based network approaches allow us to capture this interaction information. Studying such bacteria-phage interactions through community-wide networks built from inferred relationships could offer further insights into the drivers of human microbiome diversity across body sites and enable the study of human microbiome network dynamics overall.

In this study, we characterized human-associated bacterial and phage communities by their inferred relationships using three published paired virus and bacteria-dominated whole community metagenomic datasets (13, 14, 38, 39). We leveraged machine learning and graph theory techniques to establish and explore the human bacteria-phage network diversity therein. This approach built upon previous large-scale phage-bacteria network analyses by inferring interactions from metagenomic datasets, rather than culture-dependent data (33), which is limited in the scale of possible experiments and analyses.

Our metagenomic interaction inference model improved upon previous models of phage-host predictions that have utilized a variety of techniques, such as linear models to predict bacteria-phage co-occurrence using taxonomic assignments (40), and nucleotide similarity models that were applied to both whole virus genomes (41) and related clusters of whole and partial virus genomes (42). Our approach uniquely included protein interaction data and was validated based on experimentally determined positive and negative interactions (i.e. who does and does not infect whom). Through this approach we were able to provide a basic understanding of the network dynamics associated with phage and bacterial communities on and in the human body. By building and utilizing a microbiome network, we found that different people, body sites, and anatomical locations not only support distinct microbiome membership and diversity (13, 14, 38, 39, 43–45), but also support ecological communities with distinct communication structures and propensities toward community instability. Through an improved understanding of network structures across the human body, we empower future studies to investigate how these communities dynamics are influenced by disease states and the overall impact they may have on human health.

Results

Cohort Curation and Sample Processing

We studied the differences in virus-bacteria interaction networks across healthy human bodies by leveraging previously published shotgun sequence datasets of purified viral metagenomes (viromes) paired with bacteria-dominated whole community metagenomes. Our study contained three datasets that explored the impact of diet on the healthy human gut virome (14), the impact of anatomical location on the healthy human skin virome (13), and the viromes of monozygotic twins and their mothers (38, 39). We selected these datasets because their virome samples were subjected to virus-like particle (VLP) purification, which removed contaminating DNA from human cells, bacteria, etc. To this end, the publishing authors employed combinations of filtration, chloroform/DNase treatment, and cesium chloride gradients to eliminate organismal DNA (bacteria, human, fungal, etc) and thereby allow for direct assessment of both the

extracellular and fully-assembled intracellular virome **(Supplemental Figure S1 A-B)** (14, 39). Each research group reported quality control measures to ensure the purity of the virome sequence datasets, using both computational and molecular techniques, including, for example, 16S rRNA gene qPCR **(Table S1)**. These reports confirmed that the virome libraries consisted of highly purified virus genomic DNA.

The bacterial and viral sequences from these studies were quality filtered and assembled into contigs. We further grouped the related bacterial and phage contigs into operationally defined units based on their k-mer frequencies and co-abundance patterns, similar to previous reports **(Supplemental Figure S2 - S3)** (42). We referred to these operationally defined groups of related contigs as operational genomic units (OGUs). Each OGU represented a genomically similar sub-population of either bacteria or phages. Contig lengths within clusters ranged between 10^3 and $10^{5.5}$ bp **(Supplemental Figure S2 - S3)**.

We supplemented the previous study findings **(Table S1)** and found that, in light of the rigorous purification and quality control during sample collection and preparation, 77% (228 / 298 operational genomic units) still had some nucleotide similarity to a given bacterial reference genome (e-value < 10^{-25}). As absence of bacterial contamination has been confirmed **(Table S1)**, we interpret this as evidence that the majority of the gut and skin bacteriophages were temperate and thereby shared elements with bacterial reference genomes that contained similar integrated phages when sequenced–a trend previously reported (14). Additionally, we identified two OGUs as being complete phages using the stringent Virsorter phage identification algorithm (class 1 confidence group) (47).

While the whole metagenomic shotgun sequence samples were not subjected to purification, they primarily consisted of bacteria, quantified with an average viral relative abundance of 0.4% **(Table S1)** (13, 14, 38, 39). We again supplemented these findings and found that only 2% (6 / 280 operational genomic units) of bacteria had significantly strong nucleotide similarity to phage reference genomes (e-value < 10^{-25}) (13, 14, 38, 39). No OGUs were confidently identified as lytic or temperate phage OGUs in the bacterial dataset using the Virsorter algorithm (47). Together this suggests only minimal “contamination” of the bacterial OGUs.

Evaluating the Model to Predict Phage-Bacteria Interactions

We predicted which phage OGUs infected which bacterial OGUs using a random forest model trained on experimentally validated infectious relationships from six previous publications (41, 48–52). Only bacteria and phages were used in the model. The training set contained 43 diverse bacterial species and 30 diverse phage strains, including both broad and specific ranges of infection **(Supplemental Figure S4 A - B)**. While it is true that there are more known phages that infect bacteria, we were limited by the information confirming which phages do not infect certain bacteria and attempted to keep the numbers of positive and negative interactions similar. Phages with linear and circular genomes, as well as ssDNA and dsDNA genomes, were included in the analysis. Because we used DNA sequencing studies, RNA phages were not considered **(Supplemental Figure S4 C-D)**. This training set included both positive relationships (a phage infects a bacterium) and negative relationships (a phage does not infect a bacterium). This allowed us to validate the false positive and false negative rates associated with our candidate models, thereby building upon previous work that only considered positive relationships (41).

Four phage and bacterial genomic features were used in a random forest model to predict infectious relationships between bacteria and phages: 1) genome nucleotide similarities, 2) gene amino acid sequence similarities, 3) bacterial Clustered Regularly Interspaced Short Palindromic Repeat (CRISPR) spacer sequences that target phages, and 4) similarity of protein families associated with experimentally identified protein-protein interactions (53). The resulting random forest model was assessed and the area under its receiver operating characteristic (ROC) curve was 0.846, the model sensitivity was 0.829, and specificity was 0.767 **(Figure 1 A)**. The most important predictor in the model was amino acid similarity between genes, followed by nucleotide similarity of whole genomes **(Figure 1 B)**. Protein family interactions were moderately important to the model, and CRISPRs were largely uninformative, due to the minimal amount of identifiable CRISPRs in the dataset and their redundancy with the nucleotide similarity methods **(Figure 1 B)**. Approximately one third of the training set relationships yielded no score and therefore were unable to be assigned an interaction prediction **(Figure 1 C)**.

We used our random forest model to classify the relationships between bacteria and phage operational

genomic units, which were then used to build the interactive network. The master network contained the three studies as sub-networks, which themselves each contained sub-networks for each sample **(Figure 1 D)**. Metadata including study, sample ID, disease, and OGU abundance within the community were stored in the master network for parsing in downstream analyses **(Supplemental Figure S5)**. Bacterial and phage relative abundance was recorded in each sample for each OGU, and the weight of the edge connecting those OGUs was calculated as a function of those relative abundance values. The separate extraction of the phage and bacterial libraries ensured a more accurate measurement of the microbial communities, as has been outlined previously (54, 55). The master network was highly connected and contained 72,287 infectious relationships among 578 nodes, representing 298 phages and 280 bacteria. Although the network was highly connected, not all relationships were present in all samples. Relationships were weighted by the relative abundances of their associated bacteria and phages. Like the master network, the skin network exhibited a diameter of 4 (measure of graph size; the greatest number of traversed vertices required between two vertices) and included 576 (297 phages, 279 bacteria, 99.7% total) and 72,127 (99.8%) of the master network nodes and edges, respectively **(Figure 1 E - F)**. The phages and bacteria in the gut diet and twin sample sets were more sparsely related, with the diet study consisting of 89 (41 phages, 48 bacteria) nodes and 5,566 relationships, and the twin study containing 137 (36 phages, 101 bacteria) nodes and 17,250 relationships **(Figure 1 E - F)**.

Role of Diet & Obesity in Gut Microbiome Connectivity

Diet is a major environmental factor that influences resource availability and gut microbiome composition and diversity, including bacteria and phages (14, 56, 57). Previous work in isolated culture-based systems has suggested that changes in nutrient availability are associated with altered phage-bacteria network structures (30), although this has yet to be tested in humans. We therefore hypothesized that a change in diet would also be associated with a change in virome-microbiome network structure in the human gut.

We evaluated the diet-associated differences in gut virome-microbiome network structure by quantifying how central each sample's network was on average. We accomplished this by utilizing two common centrality

metrics: degree centrality and closeness centrality. Degree centrality, the simplest centrality metric, was defined as the number of connections each phage made with each bacterium. We supplemented measurements of degree centrality with measurements of closeness centrality. Closeness centrality is a metric of how close each phage or bacterium is to all of the other phages and bacteria in the network. A higher closeness centrality suggests that the effects of genetic information or altered abundance would be more impactful to all other microbes in the system. A network with higher average closeness centrality also indicates an overall greater degree of connections, which suggests a greater resilience against instability. This is because more highly connected networks are more stable as a result of pathway dependencies and the unlikelihood that a randomly removed bacteria or phage would cause major divisions across the network (30, 58). We used this information to calculate the average connectedness per sample, which was corrected for the maximum potential degree of connectedness. Unfortunately our dataset was insufficiently powered to make strong conclusions toward this hypothesis, but the data still provides an interesting "case observation" that warrants further investigation.

Using our limited sample set, we observed that the gut microbiome network structures associated with high-fat diets appeared less connected than those of low-fat diets, although a greater sample size will be required to more properly evaluate this trend **(Figure 2 A-B)**. Five subjects were available for use, all of which had matching bacteria and virome datasets and samples from 8-10 days following the initiation of their diets. High-fat diets appeared to exhibit reduced degree centrality **(Figure 2 A)**, suggesting bacteria in high-fat environments were targeted by fewer phages and that phage tropism was more restricted. High-fat diets also appeared to exhibit decreased closeness centrality **(Figure 2 B)**, indicating that bacteria and phages were more distant from other bacteria and phages in the community. This would make genetic transfer and altered abundance of a given phage or bacterium less capable of impacting other bacteria and phages within the network.

In addition to diet, we found preliminary evidence that obesity influenced network structure. This was done using the three mother samples available from the twin sample set, all of which had matching bacteria and phage samples and confirmed BMI information. The obesity-associated network appeared to have a higher

degree centrality **(Figure 2 C)**, but less closeness centrality than the healthy-associated networks **(Figure 2 D)**. These results suggested that the obesity-associated networks are less connected, having microbes further from all other microbes within the community. This again comes with the caveat that this is a case observation with too small of a sample size to make more substantial claims. This is however an area for future investigation.

Individuality of Microbial Networks

Skin and gut community membership and diversity are highly personal, with people remaining more similar to themselves than to other people over time (13, 59, 60). We therefore hypothesized that this personal conservation extended to microbiome network structure. We addressed this hypothesis by calculating the degree of dissimilarity between each subject's network, based on phage and bacteria abundance and centrality. We quantified phage and bacteria centrality within each sample graph using the weighted eigenvector centrality metric. This metric defines central phages as those that are highly abundant (A_O as defined in the methods) and infect many distinct bacteria which themselves are abundant and infected by many other phages. Similarly, bacterial centrality was defined as those bacteria that were both abundant and connected to numerous phages that were themselves connected to many bacteria. We then calculated the similarity of community networks using the weighted eigenvector centrality of all nodes between all samples. Samples with similar network structures were interpreted as having similar capacities for maintaining stability and transmitting genetic material.

We used this network dissimilarity metric to test whether microbiome network structures were more similar within people than between people over time. We found that gut microbiome network structures clustered by person (ANOSIM p-value = 0.005, R = 0.958, **Figure 3 A**). Network dissimilarity within each person over the 8-10 day sampling period was less than the average dissimilarity between that person and others, although this difference was not statistically significant (p-value = 0.125, **Figure 3 B**). Four of the five available subjects were used here because one of the subjects was not sampled at the initial time point. The lack of statistical confidence was again due to the small sample size of this dataset.

Although there was evidence for gut network conservation among individuals, we found no evidence for conservation of gut network structures within families. The gut network structures were not more similar within families (twins and their mothers; intrafamily) compared to other families (other twins and mothers; inter-family) (p-value = 0.312, **Figure 3 C**). In addition to the gut, skin microbiome network structure was strongly conserved within individuals (p-value < 0.001, **Figure 3 D**). This distribution was similar when separated by anatomical sites. Most sites were statistically significantly more conserved within individuals **(Supplemental Figure S6)**.

Association Between Environmental Stability and Network Structure Across the Human Skin Landscape

Extensive work has illustrated differences in diversity and composition of the healthy human skin microbiome between anatomical sites, including bacteria, virus, and fungal communities (13, 44, 59). These communities vary by degree of skin moisture, oil, and environmental exposure. As viruses are known to influence microbial diversity and community composition, we hypothesized that microbe-virus network structure would be specific to anatomical sites, as well. To test this, we evaluated the changes in network structure between anatomical sites within the skin dataset.

The average centrality of each sample was quantified using the weighted eigenvector centrality metric. Intermittently moist skin sites (dynamic sites that fluctuate between being moist and dry) were significantly less connected than the more stable moist and sebaceous environments (p-value < 0.001, **Figure 4 A)**. Also, skin sites that were occluded from the environment were much more highly connected than those that were constantly exposed to the environment or only intermittently occluded (p-value < 0.001, **Figure 4 B)**.

To supplement this analysis, we compared the network signatures using the centrality dissimilarity approach described above. The dissimilarity between samples was a function of shared relationships, degree of centrality, and bacteria/phage abundance. When using this supplementary approach, we found that network structures significantly clustered by moisture, sebaceous, and intermittently moist status **(Figure 4 C,E)**.

Occluded sites were significantly different from exposed and intermittently occluded sites, but there was no difference between exposed and intermittently occluded sites **(Figure 4 D,F)**. These findings provide further support that skin microbiome network structure differs significantly between skin sites.

Discussion

Foundational work has provided a baseline understanding of the human microbiome by characterizing bacterial and viral diversity across the human body (13, 14, 43–45, 61). Here, we offer an initial understanding of how phage-bacteria networks differ throughout the human body, so as to provide a baseline for future studies of how and why microbiome networks differ in disease states. We developed and implemented a network-based analytical model to evaluate the basic properties of the human microbiome through bacteria and phage relationships, instead of membership or diversity alone. This enabled the application of network theory to provide a new perspective on complex ecological communities. We utilized metrics of connectivity to model the extent to which communities of bacteria and phages interact through mechanisms such as horizontal gene transfer, modulated bacterial gene expression, and alterations in abundance.

Just as gut microbiome and virome composition and diversity are conserved in individuals (13, 43, 44, 60), gut and skin microbiome network structures were conserved within individuals over time. Gut network structure was not conserved among family members. These findings suggested that the community properties inferred from microbiome interaction network structures, such as stability (meaning a more highly connected network is more stable because a randomly removed bacteria or phage node is less likely to divide or disintegrate (30, 58) the overall network), the potential for horizontal gene transfer between members, and co-evolution of populations, were person-specific. These properties may be impacted by personal factors ranging from the body's immune system to external environmental conditions, such as climate and diet.

We observed evidence supporting the ability of environmental conditions to shape gut and skin microbiome interaction network structure by observing that diet and skin location were associated with altered network

structures. We found evidence that diet was sufficient to alter gut microbiome network connectivity, although this needs to be interpreted as a case observation, due to the small sample size. Although our sample size was small, our findings provided some preliminary evidence that high-fat diets were less connected than low-fat diets and that high-fat diets therefore may lead to less stable communities with a decreased ability for microbes to directly influence one another. We supported this finding with the observation that obesity may have been associated with decreased network connectivity. Together these findings suggest the food we eat may not only impact which microbes colonize our guts, but may also impact their interactions with infecting phages. Further work will be required to characterize these relationships with a larger cohort.

In addition to diet, the skin environment also influenced the microbiome interaction network structure. Network structure differed between environmentally exposed and occluded skin sites. The sites under greater environmental fluctuation and exposure (the exposed and intermittently exposed sites) were less connected and therefore were predicted to have a higher propensity for instability. Likewise, intermittently moist sites demonstrated less connectedness than the more stable moist and sebaceous sites. Together these data suggested that body sites under greater degrees of fluctuation harbored less connected, potentially less stable microbiomes. This points to a link between microbiome and environmental stability and warrants further investigation.

While these findings take us an important step closer to understanding the microbiome through interspecies relationships, there are caveats to and considerations regarding the approach. First, as with most classification models, the infection classification model developed and applied is only as good as its training set – in this case, the collection of experimentally-verified positive and negative infection data, where genomes of all members are fully sequenced. Large-scale experimental screens for phage and bacteria infectious interactions that report high-confidence negative interactions (i.e., no infection) are desperately needed, as they would provide more robust model training and improved model performance. Furthermore, just as we have improved on previous modeling efforts, we expect that new and creative scoring metrics will be integrated into this model to improve future performance.

Second, although our analyses utilized the best datasets currently available for our study, this work was done

retrospectively and relied on existing data up to seven years old. These archived datasets were limited by the technology and costs of the time. For example, the diet and twin studies, relied on multiple displacement amplification (MDA) in their library preparations–an approach used to overcome the large nucleic acids requirements typical of older sequencing library generation protocols. It is now known that MDA results in biases in microbial community composition (62), as well as toward ssDNA viral genomes (63, 64), thus rendering the resulting microbial and viral metagenomes largely non-quantitative. Future work that employs larger sequence datasets and that avoids the use of bias-inducing amplification steps will build on and validate our findings, as well as inform the design and interpretation of further studies.

Finally, the networks in this study were built using operational genomic units (OGUs), which represented groups of highly similar bacteria or phage genomes or clustered genome fragments. Similar clustering definition and validation methods, both computational and experimental, have been implemented in other metagenomic sequencing studies, as well (42, 65–67). These approaches could offer yet another level of sophistication to our network-based analyses. While this operationally defined clustering approach allows us to study whole community networks, our ability to make conclusions about interactions among specific phage or bacterial species or populations is inherently limited, compared to more focused, culture-based studies such as the work by Malki *et al* (68). Future work must address this limitation, e.g., through improved binning methods and deeper metagenomic shotgun sequencing, but most importantly through an improved conceptual framing of what defines ecologically and evolutionarily cohesive units for both phage and bacteria (69). Defining operational genomic units and their taxonomic underpinnings (e.g., whether OGU clusters represent genera or species) is an active area of work critical to the utility of this approach. As a first step, phylogenomic analyses have been performed to cluster cyanophage isolate genomes into informative groups using shared gene content, average nucleotide identity of shared genes, and pairwise differences between genomes (70). Such population-genetic assessment of phage evolution, coupled with the ecological implications of genome heterogeneity, will inform how to define nodes in future iterations of the ecological network developed here. Even though we are hesitant to speculate on phage host ranges at low taxonomic levels in our dataset, the data does aggree with previous reports of instances of broad phage host range (68, 71).

Together our work takes an initial step towards defining bacteria-virus interaction profiles as a characteristic of human-associated microbial communities. This approach revealed the impacts that different human environments (e.g., the skin and gut) can have on microbiome connectivity. By focusing on relationships between bacterial and viral communities, they are studied as the interacting cohorts they are, rather than as independent entities. While our developed bacteria-phage interaction framework is a novel conceptual advance, the microbiome also consists of archaea and small eukaryotes, including fungi and *Demodex* mites (1, 72)–all of which can interact with human immune cells and other non-microbial community members (73). Future work will build from our approach and include these additional community members and their diverse interactions and relationships (e.g., beyond phage-bacteria). This will result in a more robust network and a more holistic understanding of the evolutionary and ecological processes that drive the assembly and function of the human-associated microbiome.

Materials & Methods

Code Availability

A reproducible version of this manuscript written in R markdown and all of the code used to obtain and process the sequencing data is available at the following GitHub repository:

https://github.com/SchlossLab/Hannigan_ConjunctisViribus_mSystems_2017

Data Acquisition & Quality Control

Raw sequencing data and associated metadata were acquired from the NCBI sequence read archive (SRA). Supplementary metadata were acquired from the same SRA repositories and their associated manuscripts. The gut virome diet study (SRA: `SRP002424`), twin virome studies (SRA: `SRP002523`; `SRP000319`), and skin virome study (SRA: `SRP049645`) were downloaded as `.sra` files. Sequencing files were converted to `fastq` format using the `fastq-dump` tool of the NCBI SRA Toolkit (v2.2.0). Sequences were quality

trimmed using the Fastx toolkit (v0.0.14) to exclude bases with quality scores below 33 and shorter than 75 bp (74). Paired end reads were filtered to exclude sequences missing their corresponding pair using the `get_trimmed_pairs.py` script available in the source code.

Contig Assembly

Contigs were assembled using the Megahit assembly program (v1.0.6) (75). A minimum contig length of 1 kb was used. Iterative k-mer stepping began at a minimum length of 21 and progressed by 20 until 101. All other default parameters were used.

Contig Abundance Calculations

Contigs were concatenated into two master files prior to alignment, one for bacterial contigs and one for phage contigs. Sample sequences were aligned to phage or bacterial contigs using the Bowtie2 global aligner (v2.2.1) (76). We defined a mismatch threshold of 1 bp and seed length of 25 bp. Sequence abundance was calculated from the Bowtie2 output using the `calculate_abundance_from_sam.pl` script available in the source code.

Operational Genomic Unit Binning

Contigs often represent large fragments of genomes. In order to reduce redundancy and the resulting artificially inflated genomic richness within our dataset, it was important to bin contigs into operational units based on their similarity. This approach is conceptually similar to the clustering of related 16S rRNA sequences into operational taxonomic units (OTUs), although here we are clustering contigs into operational genomic units (OGUs) (61).

Contigs were clustered using the CONCOCT algorithm (v0.4.0) (77). Because of our large dataset and limits in computational efficiency, we randomly subsampled the dataset to include 25% of all samples, and used

these to inform contig abundance within the CONCOCT algorithm. CONCOCT was used with a maximum of 500 clusters, a k-mer length of four, a length threshold of 1 kb, 25 iterations, and exclusion of the total coverage variable.

OGU abundance (A_O) was obtained as the sum of the abundance of each contig (A_j) associated with that OGU. The abundance values were length corrected such that:

$$A_O = \frac{10^7 \sum_{j=1}^{k} A_j}{\sum_{j=1}^{k} L_j}$$

Where $\mathtt{L}$ is the length of each contig $\mathtt{j}$ within the OGU.

Operational Genomic Unit Identification

To confirm a lack of phage sequences in the bacterial OGU dataset, we performed blast nucleotide alignment of the bacterial OGU representative sequences using an e-value < 10^{-25}, which was stricter than the 10^{-10} threshold used in the random forest model below, against all of the phage reference genomes available in the EMBL database. We used a stricter threshold because we know there are genomic similarities between bacteria and phage OGUs from the interactive model, but we were interested in contigs with high enough similarity to references that they may indeed be from phages. We also performed the converse analysis of aligning phage OGU representative sequences to EMBL bacterial reference genomes. Finally, we ran both the phage and bacteria OGU representative sequences through the Virsorter program (1.0.3) to identify phages (all default parameters were used), using only those in the high confidence identification category "class 1" (47).

Open Reading Frame Prediction

Open reading frames (ORFs) were identified using the Prodigal program (V2.6.2) with the meta mode parameter and default settings (78).

Classification Model Creation and Validation

The classification model for predicting interactions was built using experimentally validated bacteria-phage infections or validated lack of infections from six studies (41, 48–52). Associated reference genomes were downloaded from the European Bioinformatics Institute (see details in source code). The model was created based on the four metrics listed below.

The four scores were used as parameters in a random forest model to classify bacteria and bacteriophage pairs as either having infectious interactions or not. The classification model was built using the Caret R package (v6.0.73) (79). The model was trained using five-fold cross validation with ten repeats. Pairs without scores were classified as not interacting. The model was optimized using the ROC value. The resulting model performance was plotted using the plotROC R package.

Identify Bacterial CRISPRs Targeting Phages

Clustered Regularly Interspaced Short Palindromic Repeats (CRISPRs) were identified from bacterial genomes using the PilerCR program (v1.06) (80). Resulting spacer sequences were filtered to exclude spacers shorter than 20 bp and longer than 65 bp. Spacer sequences were aligned to the phage genomes using the nucleotide BLAST algorithm with default parameters (v2.4.0) (81). The mean percent identity for each matching pair was recorded for use in our classification model.

Detect Matching Prophages within Bacterial Genomes

Temperate bacteriophages infect and integrate into their bacterial host's genome. We detected integrated phage elements within bacterial genomes by aligning phage genomes to bacterial genomes using the nucleotide BLAST algorithm and a minimum e-value of 1e-10. The resulting bitscore of each alignment was recorded for use in our classification model.

Identify Shared Genes Between Bacteria and Phages

As a result of gene transfer or phage genome integration during infection, phages may share genes with their bacterial hosts, providing us with evidence of phage-host pairing. We identified shared genes between bacterial and phage genomes by assessing amino acid similarity between the genes using the Diamond protein alignment algorithm (v0.7.11.60) (82). The mean alignment bitscores for each genome pair were recorded for use in our classification model.

Protein - Protein Interactions

The final method used for predicting infectious interactions between bacteria and phages was the detection of pairs of genes whose proteins are known to interact. We assigned bacterial and phage genes to protein families by aligning them to the Pfam database using the Diamond protein alignment algorithm. We then identified which pairs of proteins were predicted to interact using the Pfam interaction information within the Intact database (53). The mean bitscores of the matches between each pair were recorded for use in the classification model.

Interaction Network Construction

The bacteria and phage operational genomic units (OGUs) were scored using the same approach as outlined above. The infectious pairings between bacteria and phage OGUs were classified using the random forest model described above. The predicted infectious pairings and all associated metadata were used to populate a graph database using Neo4j graph database software (v2.3.1) (83). This network was used for downstream community analysis.

Centrality Analysis

We quantified the centrality of graph vertices using three different metrics, each of which provided different information graph structure. When calculating these values, let $G(V, E)$ be an undirected, unweighted graph with $|V| = n$ nodes and $|E| = m$ edges. Also, let $\mathbf{A}$ be its corresponding adjacency matrix with entries

$a_{ij} = 1$ if nodes V_i and V_j are connected via an edge, and $a_{ij} = 0$ otherwise.

Briefly, the **closeness centrality** of node V_i is calculated taking the inverse of the average length of the shortest paths (d) between nodes V_i and all the other nodes V_j. Mathematically, the closeness centrality of node V_i is given as:

$$C_C\left(V_i\right) = \left(\sum_{j=1}^{n} d\left(V_i, V_j\right)\right)^{-1}$$

The distance between nodes (d) was calculated as the shortest number of edges required to be traversed to move from one node to another.

Intuitively, the **degree centrality** of node V_i is defined as the number of edges that are incident to that node:

$$C_D\left(V_i\right) = \sum_{j=1}^{n} a_{ij}$$

where a_{ij} is the ij^{th} entry in the adjacency matrix $\mathbf{A}$.

The eigenvector centrality of node V_i is defined as the i^{th} value in the first eigenvector of the associated adjacency matrix $\mathbf{A}$. Conceptually, this function results in a centrality value that reflects the connections of the vertex, as well as the centrality of its neighboring vertices.

The **centralization** metric was used to assess the average centrality of each sample graph $\mathbf{G}$. Centralization was calculated by taking the sum of each vertex V_i's centrality from the graph maximum centrality C_w, such that:

$$C\left(G\right) = \frac{\sum_{i=1}^{n} Cw - c\left(V_i\right)}{T}$$

The values were corrected for uneven graph sizes by dividing the centralization score by the maximum theoretical centralization (T) for a graph with the same number of vertices.

Degree and closeness centrality were calculated using the associated functions within the igraph R package (v1.0.1) (84).

Network Relationship Dissimilarity

We assessed similarity between graphs by evaluating the shared centrality of their vertices, as has been done previously. More specifically, we calculated the dissimilarity between graphs G_i and G_j using the Bray-Curtis dissimilarity metric and eigenvector centrality values such that:

$$B\left(G_i, G_j\right) = 1 - \frac{2C_{ij}}{C_i + C_j}$$

Where C_{ij} is the sum of the lesser centrality values for those vertices shared between graphs, and C_i and C_j are the total number of vertices found in each graph. This allows us to calculate the dissimilarity between graphs based on the shared centrality values between the two graphs.

Statistics and Comparisons

Differences in intrapersonal and interpersonal network structure diversity, based on multivariate data, were calculated using an analysis of similarity (ANOSIM). Statistical significance of univariate Eigenvector centrality differences were calculated using a paired Wilcoxon test.

Statistical significance of differences in univariate eigenvector centrality measurements of skin virome-microbiome networks were calculated using a pairwise Wilcoxon test, corrected for multiple hypothesis tests using the Holm correction method. Multivariate eigenvector centrality was measured as the mean differences between cluster centroids, with statistical significance measured using an ANOVA and post hoc Tukey test.

Acknowledgments

We thank the members of the Schloss lab for their underlying contributions. We thank the authors of the original studies for making their data and metadata publicly available and understandable. We also thank the participants in the studies.

Funding Information

GDH was supported in part by the Molecular Mechanisms in Microbial Pathogenesis Training Program (T32 AI007528). GDH and PDS were supported in part by funding from the NIH (P30DK034933, U19AI09087, and U01AI124255).

Disclosure Declaration

The authors report no conflicts of interest.

Figures

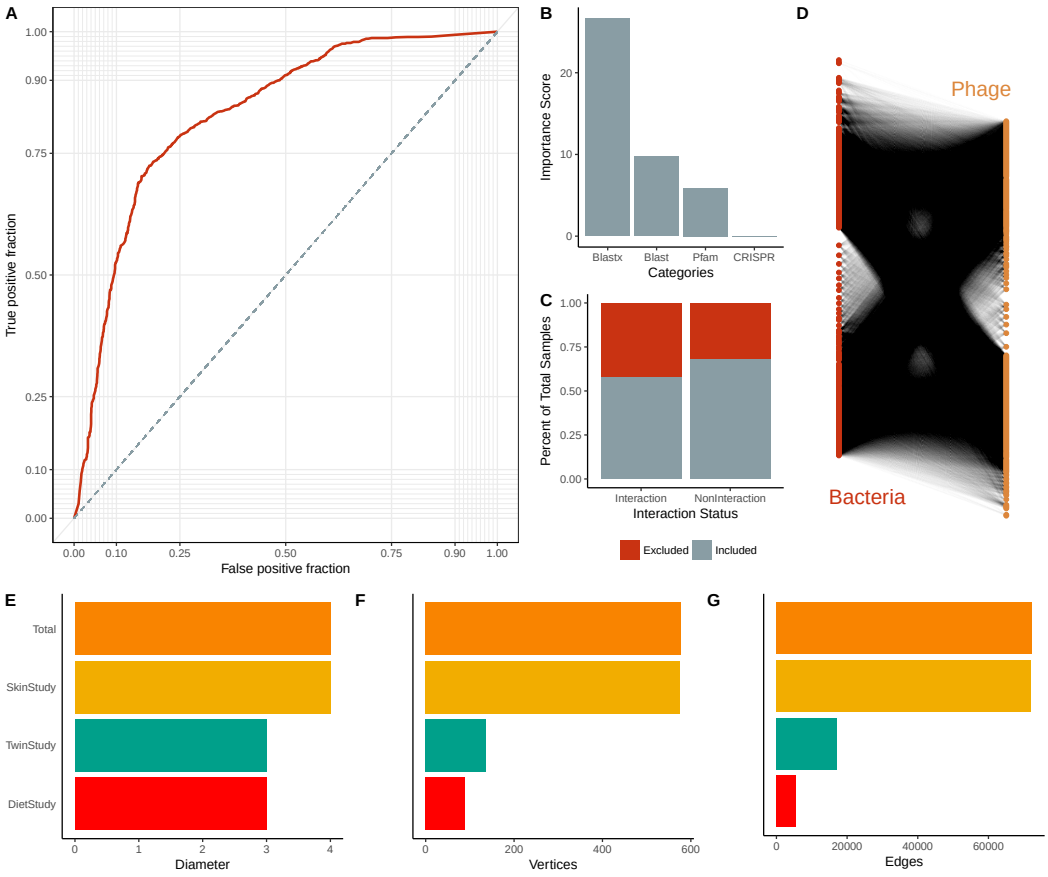

Figure 1: **Summary of Multi-Study Network Model.** *(A) Average ROC curve used to create the microbiome-virome infection prediction model. (B) Importance scores associated with the metrics used in the random forest model to predict relationships between bacteria and phages. The importance score is defined as the mean decrease in accuracy of the model when a feature (e.g. Pfam) is excluded. Features include the local gene alignments between bacteria and phage genes (denoted* `blastx`*; the blastx algorithm in Diamond aligner), local genome nucleotide alignments between bacteria and phage OGUs, presence of experimentally validated protein family domains (Pfams) between phage and bacteria OGUs, and CRISPR targeting of bacteria toward phages (CRISPR). (C) Proportions of samples included (gray) and excluded (red) in the model. Samples were excluded from the model because they did not yield any scores. Those interactions without scores were automatically classified as not having interactions. (D) Bipartite visualization of the resulting phage-bacteria network. Phage OGUs are presented in orange, bacteria OGUs in red, and their interaction edges are represented as connecting lines. This network includes information from all three published studies. (E) Network diameter (measure of graph size; the greatest number of traversed vertices required between two vertices), (F) number of vertices, and (G) number of edges (relationships) for the total network (orange) and the individual study sub-networks (diet study = red, skin study = yellow, twin study = green).*

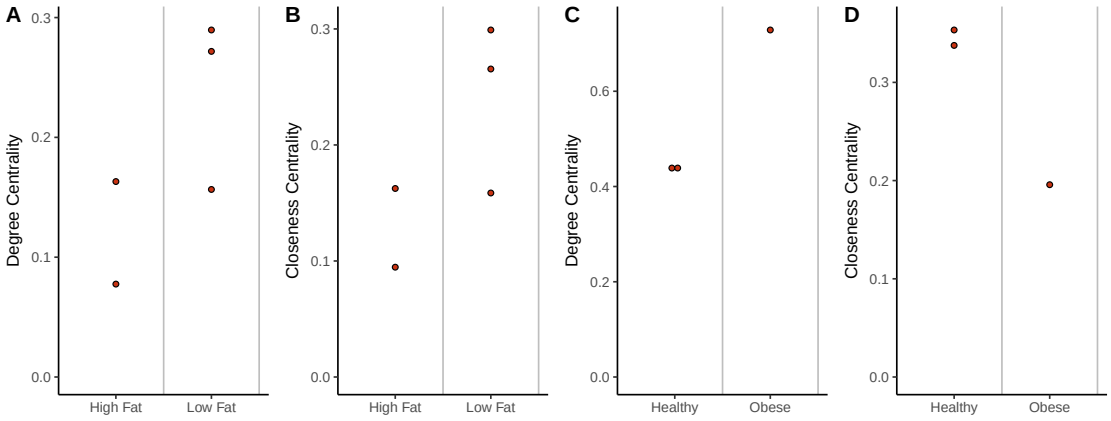

Figure 2: **Impact of Diet and Obesity on Gut Network Structure.** *(A) Quantification of average degree centrality (number of edges per node) and (B) closeness centrality (average distance from each node to every other node) of gut microbiome networks of subjects limited to exclusively high-fat or low-fat diets. Each point represents the centrality from a human subject stool sample that was collected 8-10 days following the beginning of their defined diet. There are five samples here, compared to the four in figure 3, because one of the was only sampled post-diet, providing us data for this analysis but not allowing us to compare to a baseline for figure 3. (C) Quantification of average degree centrality and (D) closeness centrality between obese and healthy adult women from the Twin gut study. Each point represents a stool sample taken from one of the three adult woman confirmed as obese or healthy and with matching virus and bacteria data.*

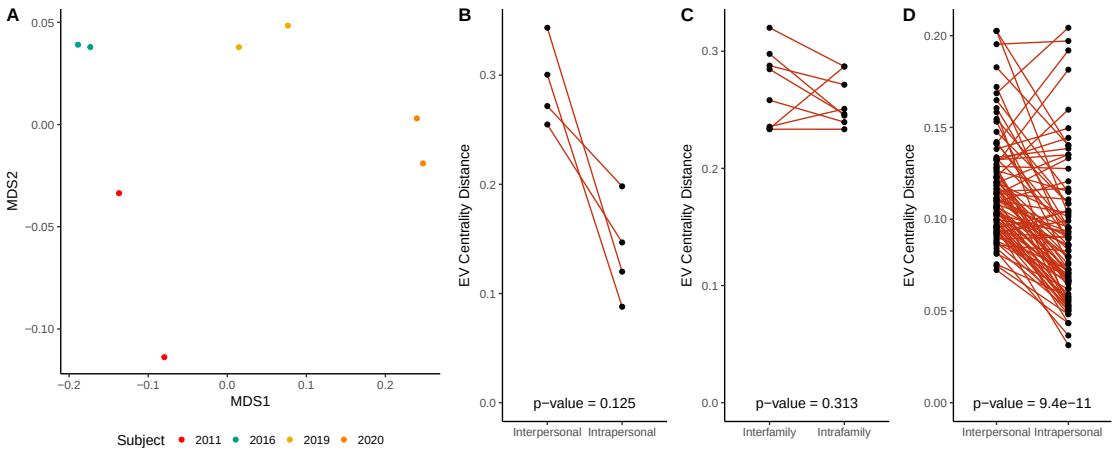

Figure 3: **Intrapersonal vs Interpersonal Network Dissimilarity Across Different Human Systems.** *(A) NMDS ordination illustrating network dissimilarity between subjects over time. Each sample is colored by subject, with each colored sample pair collected 8-10 days apart. Dissimilarity was calculated using the Bray-Curtis metric based on abundance weighted eigenvector centrality signatures, with a greater distance representing greater dissimilarity in bacteria and phage centrality and abundance. Only four subjects were included here, compared to the five used in figure 2, because one of the subjects was missing the inital sampling time point and therefore lacked temporal sampling. (B) Quantification of gut network dissimilarity within the same subject over time (intrapersonal) and the mean dissimilarity between the subject of interest and all other subjects (interpersonal). The p-value is provided near the bottom of the figure. (C) Quantification of gut network dissimilarity within subjects from the same family (intrafamily) and the mean dissimilarity between subjects within a family and those of other families (interfamily). Each point represents the inter-family and intra-family dissimilarity of a twin or mother that was sampled over time. (D) Quantification of skin network dissimilarity within the same subject and anatomical location over time (intrapersonal) and the mean dissimilarity between the subject of interest and all other subjects at the same time and the same anatomical location (interpersonal). All p-values were calculated using a paired Wilcoxon test.*

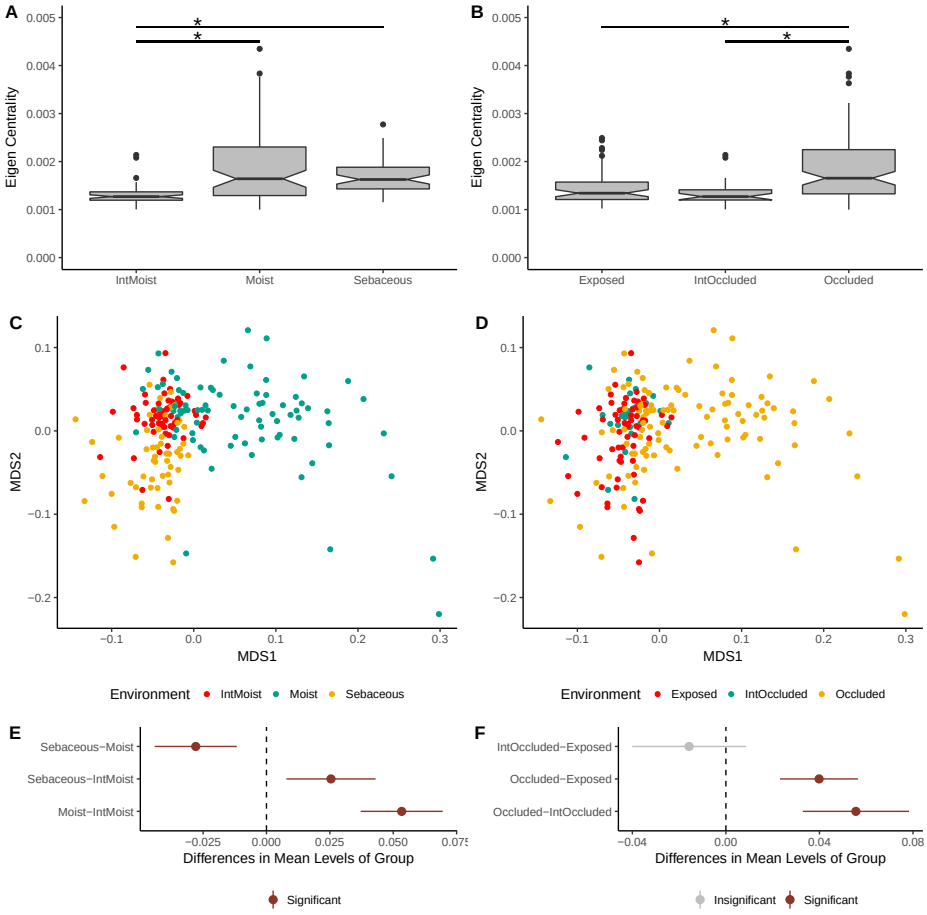

Figure 4: **Impact of Skin Micro-Environment on Microbiome Network Structure.** *(A) Notched box-plot depicting differences in average eigenvector centrality between moist, intermittently moist, and sebaceous skin sites and (B) occluded, intermittently occluded, and exposed sites. Notched box-plots were created using ggplot2 and show the median (center line), the inter-quartile range (IQR; upper and lower boxes), the highest and lowest value within 1.5 * IQR (whiskers), outliers (dots), and the notch which provides an approximate 95% confidence interval as defined by 1.58 * IQR / sqrt(n). Sample sizes for each group were: Moist = 81, Sebaceous = 56, IntMoist = 56, Occluded = 106, Exposed = 61, IntOccluded = 26. (C) NMDS ordination depicting the differences in skin microbiome network structure between skin moisture levels and (D) occlusion. Samples are colored by their environment and their dissimilarity to other samples was calculated as described in figure 3. (E) The statistical differences of networks between moisture and (F) occlusion status were quantified with an anova and post hoc Tukey test. Cluster centroids are represented by dots and the extended lines represent the associated 95% confidence intervals. Significant comparisons (p-value < 0.05) are colored in red, and non-significant comparisons are gray.*

Supplemental Figures

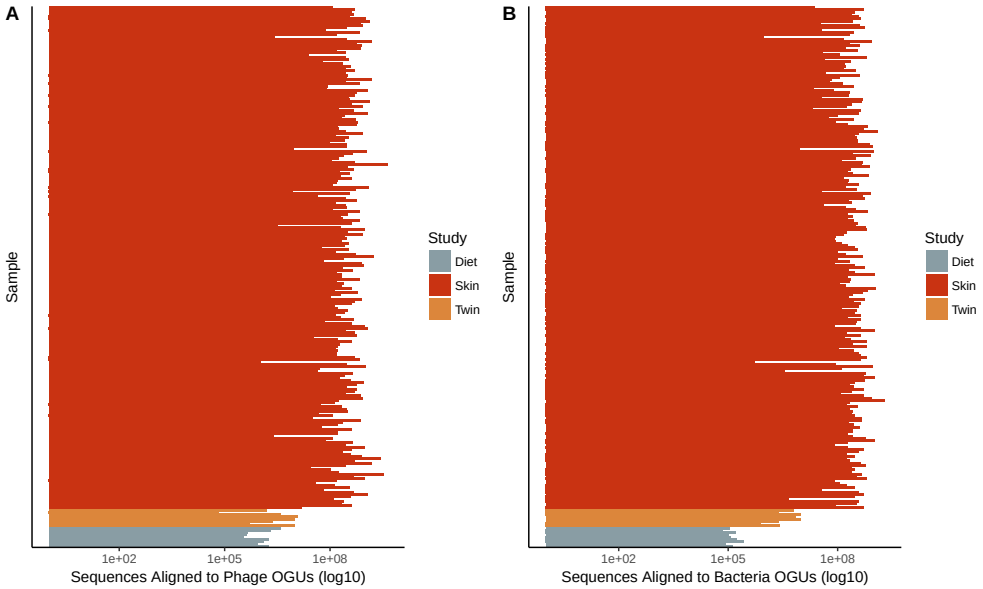

Figure S1: **Sequencing Depth Summary.** *Number of sequences that aligned to (A) Phage and (B) Bacteria operational genomic units per sample and colored by study.*

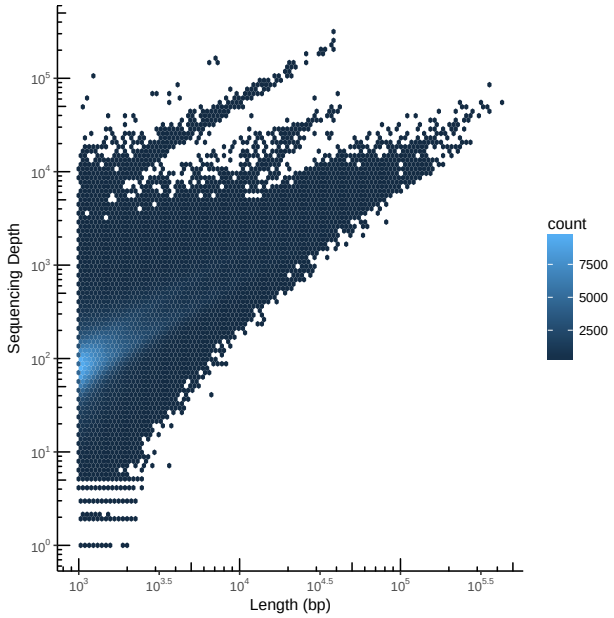

Figure S2: **Contig Summary Statistics.** *Scatter plot heat map with each hexagon representing the abundance of contigs. Contigs are organized by length on the x-axis and the number of aligned sequences on the y-axis.*

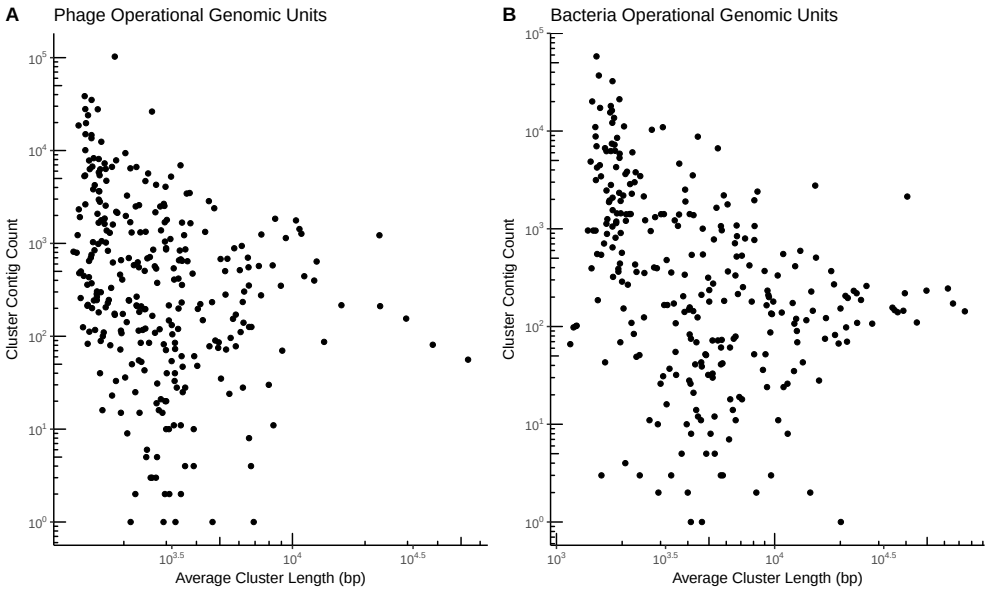

Figure S3: **Operational Genomic Unit Summary Statistics.** *Scatter plot with operational genomic unit clusters organized by average contig length within the cluster on the x-axis and the number of contigs in the cluster on the y-axis. Operational genomic units of (A) bacteriophages and (B) bacteria are shown.*

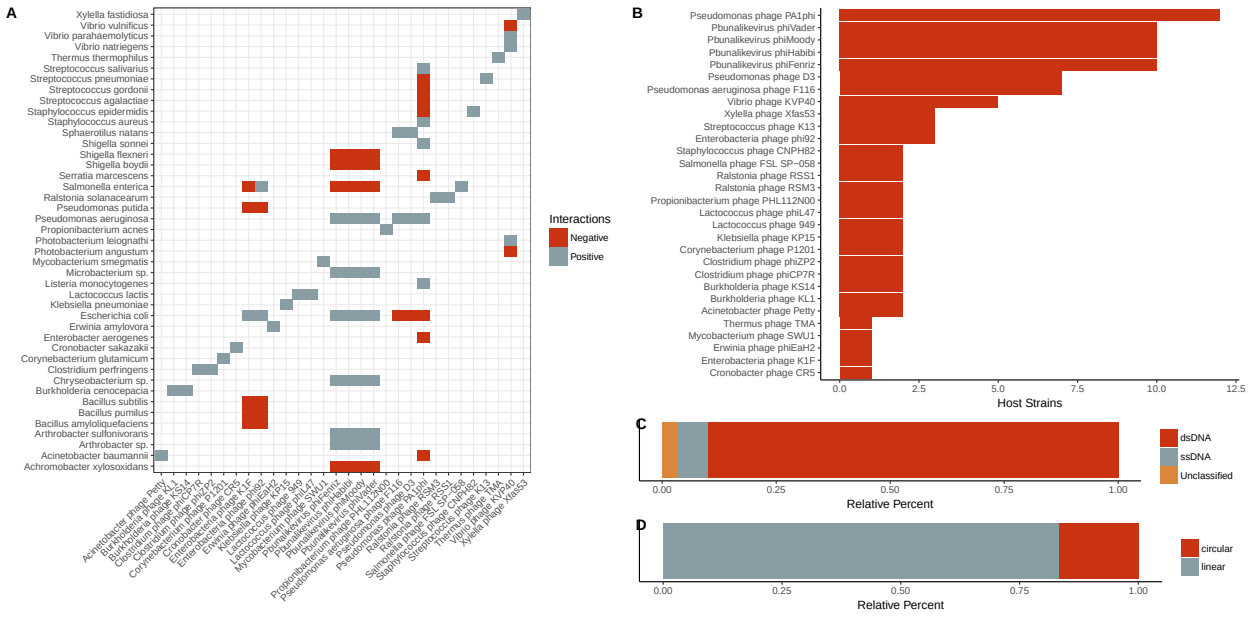

Figure S4: **Summary information of validation dataset used in the interaction predictive model.** *A) Categorical heat-map highlighting the experimentally validated positive and negative interactions. Only bacteria species are shown, which represent multiple reference strains. Phages are labeled on the x-axis and bacteria are labeled on the y-axis. B) Quantification of bacterial host strains known to exist for each phage. C) Genome strandedness and D) linearity of the phage reference genomes used for the dataset.*

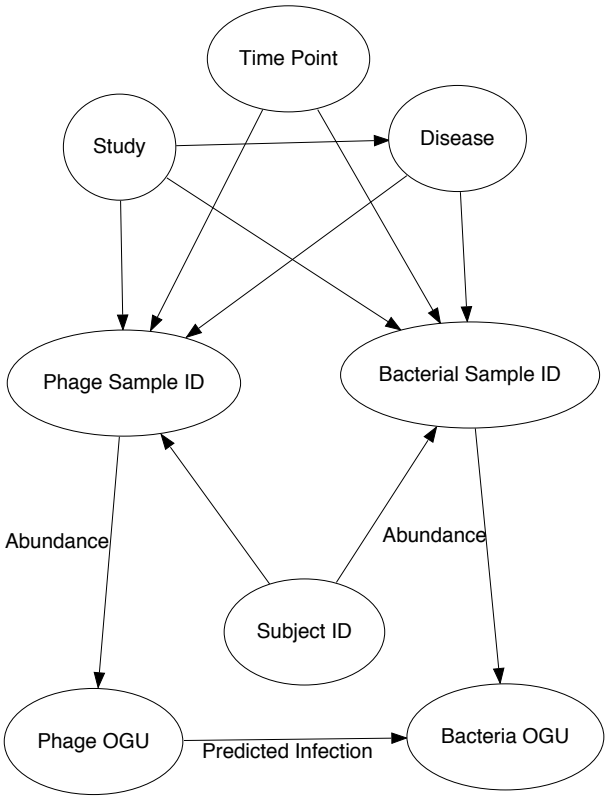

Figure S5: **Structure of the interactive network.** *Metadata relationships to samples (Phage Sample ID and Bacteria Sample ID) included the associated time point, the study, the subject the sample was taken from, and the associated disease. Infectious interactions were recorded between phage and bacteria operational genomic units (OGUs). Sequence count abundance for each OGU within each sample was also recorded.*

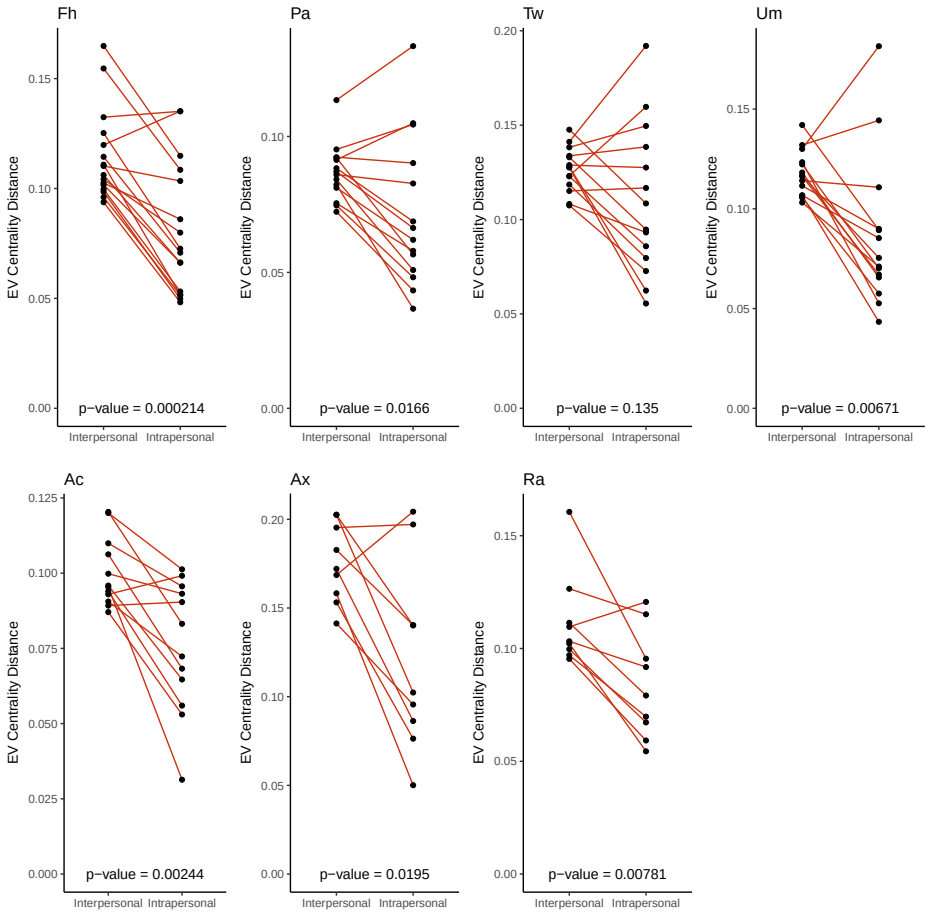

Figure S6: **Intrapersonal vs Interpersonal Dissimilarity of the Skin.** *Quantification of skin network dissimilarity within the same subject and anatomical location over time (intrapersonal) and the mean dissimilarity between the subject of interest and all other subjects at the same time and the same anatomical location (interpersonal), separated by each anatomical site (forehead [Fh], palm [Pa], toe web [Tw], umbilicus [Um], antecubital fossa [Ac], axilla [Ax], and retroauricular crease [Ra]). P-value was calculated using a paired Wilcoxon test.*

Supplemental Tables

Table S1: Summary of the primary quality control measures reported in the original publications of the viromes used in this current study.

Study	Citation	Virome Quality Control Measures
Diet & the Gut Virome	Minot, 2011	• 16S rRNA gene qPCR revealed reduction in bacterial DNA of at least 10,000X. • Alignment of shotgun sequences revealed 35X reduction in 16S rRNA gene alignments in virome compared to bacteria shotgun. • Electron microscopy and nucleic acid stain techniques visually confirmed lack of bacteria in virome samples.
Skin Virome	Hannigan, 2015	• Significant reduction in reads mapping to 16S rRNA gene sequence, compared to bacteria shotgun dataset. • Significant reduction in reads mapping to human genome, compared to bacteria shotgun dataset. • Average viral relative abundance of 0.4% in bacterial shotgun dataset.
Twin Gut Virome	Reyes, 2010	• Confirmation that 2.5% of bacterial shotgun reads mapped to virome, and 76% of virome reads matched the shotgun 2.5%.

References

1. **Hannigan GD**, **Grice EA**. 2013. Microbial Ecology of the Skin in the Era of Metagenomics and Molecular Microbiology. Cold Spring Harbor Perspectives in Medicine **3**:a015362–a015362.

2. **Hannigan GD**, **Hodkinson BP**, **McGinnis K**, **Tyldsley AS**, **Anari JB**, **Horan AD**, **Grice EA**, **Mehta S**. 2014. Culture-independent pilot study of microbiota colonizing open fractures and association with severity, mechanism, location, and complication from presentation to early outpatient follow-up. Journal of Orthopaedic Research **32**:597–605.

3. **Loesche M**, **Gardner SE**, **Kalan L**, **Horwinski J**, **Zheng Q**, **Hodkinson BP**, **Tyldsley AS**, **Franciscus CL**, **Hillis SL**, **Mehta S**, **Margolis DJ**, **Grice EA**. 2016. Temporal stability in chronic wound microbiota is associated with poor healing. Journal of Investigative Dermatology.

4. **He Q**, **Li X**, **Liu C**, **Su L**, **Xia Z**, **Li X**, **Li Y**, **Li L**, **Yan T**, **Feng Q**, **Xiao L**. 2016. Dysbiosis of the fecal microbiota in the TNBS-induced Crohn's disease mouse model. Applied Microbiology and Biotechnology 1–10.

5. **Norman JM**, **Handley SA**, **Baldridge MT**, **Droit L**, **Liu CY**, **Keller BC**, **Kambal A**, **Monaco CL**, **Zhao G**, **Fleshner P**, **Stappenbeck TS**, **McGovern DPB**, **Keshavarzian A**, **Mutlu EA**, **Sauk J**, **Gevers D**, **Xavier RJ**, **Wang D**, **Parkes M**, **Virgin HW**. 2015. Disease-specific alterations in the enteric virome in inflammatory bowel disease. Cell **160**:447–460.

6. **Seekatz AM**, **Rao K**, **Santhosh K**, **Young VB**. 2016. Dynamics of the fecal microbiome in patients with recurrent and nonrecurrent Clostridium difficile infection. Genome medicine **8**:47.

7. **Zackular JP**, **Rogers MAM**, **Ruffin MT**, **Schloss PD**. 2014. The human gut microbiome as a screening tool for colorectal cancer. Cancer prevention research (Philadelphia, Pa) **7**:1112–1121.

8. **Baxter NT**, **Zackular JP**, **Chen GY**, **Schloss PD**. 2014. Structure of the gut microbiome following colonization with human feces determines colonic tumor burden. Microbiome **2**:20.

9. **Manrique P**, **Bolduc B**, **Walk ST**, **Oost J van der**, **Vos WM de**, **Young MJ**. 2016. Healthy human gut

phageome. Proceedings of the National Academy of Sciences of the United States of America 201601060.

10. **Ly M**, **Abeles SR**, **Boehm TK**, **Robles-Sikisaka R**, **Naidu M**, **Santiago-Rodriguez T**, **Pride DT**. 2014. Altered Oral Viral Ecology in Association with Periodontal Disease. mBio **5**:e01133–14–e01133–14.

11. **Modi SR**, **Lee HH**, **Spina CS**, **Collins JJ**. 2013. Antibiotic treatment expands the resistance reservoir and ecological network of the phage metagenome. Nature **499**:219–222.

12. **Monaco CL**, **Gootenberg DB**, **Zhao G**, **Handley SA**, **Ghebremichael MS**, **Lim ES**, **Lankowski A**, **Baldridge MT**, **Wilen CB**, **Flagg M**, **Norman JM**, **Keller BC**, **Luévano JM**, **Wang D**, **Boum Y**, **Martin JN**, **Hunt PW**, **Bangsberg DR**, **Siedner MJ**, **Kwon DS**, **Virgin HW**. 2016. Altered Virome and Bacterial Microbiome in Human Immunodeficiency Virus-Associated Acquired Immunodeficiency Syndrome. Cell Host and Microbe **19**:311–322.

13. **Hannigan GD**, **Meisel JS**, **Tyldsley AS**, **Zheng Q**, **Hodkinson BP**, **SanMiguel AJ**, **Minot S**, **Bushman FD**, **Grice EA**. 2015. The Human Skin Double-Stranded DNA Virome: Topographical and Temporal Diversity, Genetic Enrichment, and Dynamic Associations with the Host Microbiome. mBio **6**:e01578–15.

14. **Minot S**, **Sinha R**, **Chen J**, **Li H**, **Keilbaugh SA**, **Wu GD**, **Lewis JD**, **Bushman FD**. 2011. The human gut virome: Inter-individual variation and dynamic response to diet. Genome Research **21**:1616–1625.

15. **Santiago-Rodriguez TM**, **Ly M**, **Bonilla N**, **Pride DT**. 2015. The human urine virome in association with urinary tract infections. Frontiers in Microbiology **6**:14.

16. **Abeles SR**, **Ly M**, **Santiago-Rodriguez TM**, **Pride DT**. 2015. Effects of Long Term Antibiotic Therapy on Human Oral and Fecal Viromes. PLOS ONE **10**:e0134941.

17. **Abeles SR**, **Robles-Sikisaka R**, **Ly M**, **Lum AG**, **Salzman J**, **Boehm TK**, **Pride DT**. 2014. Human oral viruses are personal, persistent and gender-consistent 1–15.

18. **Haerter JO**, **Mitarai N**, **Sneppen K**. 2014. Phage and bacteria support mutual diversity in a narrowing staircase of coexistence. The ISME Journal **8**:2317–2326.

19. **Lindell D**, **Jaffe JD**, **Johnson ZI**, **Church GM**, **Chisholm SW**. 2005. Photosynthesis genes in marine

524 viruses yield proteins during host infection. Nature **438**:86–89.

525 20. **Tyler JS**, **Beeri K**, **Reynolds JL**, **Alteri CJ**, **Skinner KG**, **Friedman JH**, **Eaton KA**, **Friedman DI**. 2013.
526 Prophage induction is enhanced and required for renal disease and lethality in an EHEC mouse model. PLoS
527 Pathogens **9**:e1003236.

528 21. **Hargreaves KR**, **Kropinski AM**, **Clokie MR**. 2014. Bacteriophage behavioral ecology: How phages alter
529 their bacterial host's habits. Bacteriophage **4**:e29866.

530 22. **Moon BY**, **Park JY**, **Hwang SY**, **Robinson DA**, **Thomas JC**, **Fitzgerald JR**, **Park YH**, **Seo KS**. 2015.
531 Phage-mediated horizontal transfer of a Staphylococcus aureus virulence-associated genomic island.
532 Scientific Reports **5**:9784.

533 23. **Modi SR**, **Lee HH**, **Spina CS**, **Collins JJ**. 2013. Antibiotic treatment expands the resistance reservoir
534 and ecological network of the phage metagenome. Nature **499**:219–222.

535 24. **Ogg JE**, **Timme TL**, **Alemohammad MM**. 1981. General Transduction in Vibrio cholerae. Infection and
536 Immunity **31**:737–741.

537 25. **Frost LS**, **Leplae R**, **Summers AO**, **Toussaint A**. 2005. Mobile genetic elements: the agents of open
538 source evolution. Nature Reviews Microbiology **3**:722–732.

539 26. **Koskella B**, **Brockhurst MA**. 2014. Bacteria-phage coevolution as a driver of ecological and evolutionary
540 processes in microbial communities. FEMS Microbiology Reviews **38**:916–931.

541 27. **Jover LF**, **Effler TC**, **Buchan A**, **Wilhelm SW**, **Weitz JS**. 2014. The elemental composition of virus
542 particles: implications for marine biogeochemical cycles. Nature Reviews Microbiology **12**:519–528.

543 28. **Harcombe WR**, **Bull JJ**. 2005. Impact of phages on two-species bacterial communities. Applied and
544 Environmental Microbiology **71**:5254–5259.

545 29. **Middelboe M**, **Hagström A**, **Blackburn N**, **Sinn B**, **Fischer U**, **Borch NH**, **Pinhassi J**, **Simu K**, **Lorenz**
546 **MG**. 2001. Effects of Bacteriophages on the Population Dynamics of Four Strains of Pelagic Marine Bacteria.

547 Microbial Ecology **42**:395–406.

548 30. **Poisot T**, **Lepennetier G**, **Martinez E**, **Ramsayer J**, **Hochberg ME**. 2011. Resource availability affects
549 the structure of a natural bacteriabacteriophage community. Biology letters **7**:201–204.

550 31. **Thompson RM**, **Brose U**, **Dunne JA**, **Hall RO**, **Hladyz S**, **Kitching RL**, **Martinez ND**, **Rantala H**,
551 **Romanuk TN**, **Stouffer DB**, **Tylianakis JM**. 2012. Food webs: reconciling the structure and function of
552 biodiversity. Trends in ecology & evolution **27**:689–697.

553 32. **Moebus K**, **Nattkemper H**. 1981. Bacteriophage sensitivity patterns among bacteria isolated from marine
554 waters. Helgoländer Meeresuntersuchungen **34**:375–385.

555 33. **Flores CO**, **Valverde S**, **Weitz JS**. 2013. Multi-scale structure and geographic drivers of cross-infection
556 within marine bacteria and phages. The ISME Journal **7**:520–532.

557 34. **Poisot T**, **Canard E**, **Mouillot D**, **Mouquet N**, **Gravel D**. 2012. The dissimilarity of species interaction
558 networks. Ecology letters **15**:1353–1361.

559 35. **Poisot T**, **Stouffer D**. 2016. How ecological networks evolve. bioRxiv.

560 36. **Flores CO**, **Meyer JR**, **Valverde S**, **Farr L**, **Weitz JS**. 2011. Statistical structure of host-phage interactions.
561 Proceedings of the National Academy of Sciences of the United States of America **108**:E288–97.

562 37. **Jover LF**, **Flores CO**, **Cortez MH**, **Weitz JS**. 2015. Multiple regimes of robust patterns between network
563 structure and biodiversity. Scientific Reports **5**:17856.

564 38. **Reyes A**, **Haynes M**, **Hanson N**, **Angly FE**, **Heath AC**, **Rohwer F**, **Gordon JI**. 2010. Viruses in the
565 faecal microbiota of monozygotic twins and their mothers. Nature **466**:334–338.

566 39. **Turnbaugh PJ**, **Hamady M**, **Yatsunenko T**, **Cantarel BL**, **Duncan A**, **Ley RE**, **Sogin ML**, **Jones WJ**, **Roe**
567 **BA**, **Affourtit JP**, **Egholm M**, **Henrissat B**, **Heath AC**, **Knight R**, **Gordon JI**. 2009. A core gut microbiome
568 in obese and lean twins. Nature **457**:480–484.

569 40. **Lima-Mendez G**, **Faust K**, **Henry N**, **Decelle J**, **Colin S**, **Carcillo F**, **Chaffron S**, **Ignacio-Espinosa JC**,
570 **Roux S**, **Vincent F**, **Bittner L**, **Darzi Y**, **Wang J**, **Audic S**, **Berline L**, **Bontempi G**, **Cabello AM**, **Coppola**

L, **Cornejo-Castillo FM**, **d'Ovidio F**, **De Meester L**, **Ferrera I**, **Garet-Delmas M-J**, **Guidi L**, **Lara E**, **Pesant S**, **Royo-Llonch M**, **Salazar G**, **Sánchez P**, **Sebastian M**, **Souffreau C**, **Dimier C**, **Picheral M**, **Searson S**, **Kandels-Lewis S**, **Tara Oceans Coordinators**, **Gorsky G**, **Not F**, **Ogata H**, **Speich S**, **Stemmann L**, **Weissenbach J**, **Wincker P**, **Acinas SG**, **Sunagawa S**, **Bork P**, **Sullivan MB**, **Karsenti E**, **Bowler C**, **Vargas C de**, **Raes J**. 2015. Ocean plankton. Determinants of community structure in the global plankton interactome. Science **348**:1262073–1262073.

41. **Edwards RA**, **McNair K**, **Faust K**, **Raes J**, **Dutilh BE**. 2015. Computational approaches to predict bacteriophage-host relationships. FEMS Microbiology Reviews **40**:258–272.

42. **Roux S**, **Brum JR**, **Dutilh BE**, **Sunagawa S**, **Duhaime MB**, **Loy A**, **Poulos BT**, **Solonenko N**, **Lara E**, **Poulain J**, **Pesant S**, **Kandels-Lewis S**, **Dimier C**, **Picheral M**, **Searson S**, **Cruaud C**, **Alberti A**, **Duarte CM**, **Gasol JM**, **Vaqué D**, **Tara Oceans Coordinators**, **Bork P**, **Acinas SG**, **Wincker P**, **Sullivan MB**. 2016. Ecogenomics and potential biogeochemical impacts of globally abundant ocean viruses. Nature **537**:689–693.

43. **Grice EA**, **Kong HH**, **Conlan S**, **Deming CB**, **Davis J**, **Young AC**, **NISC Comparative Sequencing Program**, **Bouffard GG**, **Blakesley RW**, **Murray PR**, **Green ED**, **Turner ML**, **Segre JA**. 2009. Topographical and Temporal Diversity of the Human Skin Microbiome. Science **324**:1190–1192.

44. **Findley K**, **Oh J**, **Yang J**, **Conlan S**, **Deming C**, **Meyer JA**, **Schoenfeld D**, **Nomicos E**, **Park M**, **NIH Intramural Sequencing Center Comparative Sequencing Program**, **Kong HH**, **Segre JA**. 2013. Topographic diversity of fungal and bacterial communities in human skin. Nature 1–6.

45. **Costello EK**, **Lauber CL**, **Hamady M**, **Fierer N**, **Gordon JI**, **Knight R**. 2009. Bacterial community variation in human body habitats across space and time. Science **326**:1694–1697.

46. **Consortium THMP**. 2012. A framework for human microbiome research. Nature **486**:215–221.

47. **Roux S**, **Enault F**, **Hurwitz BL**, **Sullivan MB**. 2015. VirSorter: mining viral signal from microbial genomic data. PeerJ **3**:e985–20.

48. **Jensen EC**, **Schrader HS**, **Rieland B**, **Thompson TL**, **Lee KW**, **Nickerson KW**, **Kokjohn TA**.

1998. Prevalence of broad-host-range lytic bacteriophages of Sphaerotilus natans, Escherichia coli, and Pseudomonas aeruginosa. Applied and Environmental Microbiology **64**:575–580.

49. **Malki K**, **Kula A**, **Bruder K**, **Sible E**. 2015. Bacteriophages isolated from Lake Michigan demonstrate broad host-range across several bacterial phyla. Virology.

50. **Schwarzer D**, **Buettner FFR**, **Browning C**, **Nazarov S**, **Rabsch W**, **Bethe A**, **Oberbeck A**, **Bowman VD**, **Stummeyer K**, **Mühlenhoff M**, **Leiman PG**, **Gerardy-Schahn R**. 2012. A multivalent adsorption apparatus explains the broad host range of phage phi92: a comprehensive genomic and structural analysis. Journal of Virology **86**:10384–10398.

51. **Kim S**, **Rahman M**, **Seol SY**, **Yoon SS**, **Kim J**. 2012. Pseudomonas aeruginosa bacteriophage PA1Ø requires type IV pili for infection and shows broad bactericidal and biofilm removal activities. Applied and Environmental Microbiology **78**:6380–6385.

52. **Matsuzaki S**, **Tanaka S**, **Koga T**, **Kawata T**. 1992. A Broad-Host-Range Vibriophage, KVP40, Isolated from Sea Water. Microbiology and Immunology **36**:93–97.

53. **Orchard S**, **Ammari M**, **Aranda B**, **Breuza L**, **Briganti L**, **Broackes-Carter F**, **Campbell NH**, **Chavali G**, **Chen C**, **del-Toro N**, **Duesbury M**, **Dumousseau M**, **Galeota E**, **Hinz U**, **Iannuccelli M**, **Jagannathan S**, **Jimenez R**, **Khadake J**, **Lagreid A**, **Licata L**, **Lovering RC**, **Meldal B**, **Melidoni AN**, **Milagros M**, **Peluso D**, **Perfetto L**, **Porras P**, **Raghunath A**, **Ricard-Blum S**, **Roechert B**, **Stutz A**, **Tognolli M**, **Roey K van**, **Cesareni G**, **Hermjakob H**. 2014. The MIntAct project–IntAct as a common curation platform for 11 molecular interaction databases. Nucleic Acids Research **42**:D358–63.

54. **Kleiner M**, **Hooper LV**, **Duerkop BA**. 2015. Evaluation of methods to purify virus-like particles for metagenomic sequencing of intestinal viromes. BMC Genomics **16**:7.

55. **Meisel JS**, **Hannigan GD**, **Tyldsley AS**, **SanMiguel AJ**, **Hodkinson BP**, **Zheng Q**, **Grice EA**. 2016. Skin microbiome surveys are strongly influenced by experimental design. Journal of Investigative Dermatology.

56. **Turnbaugh PJ**, **Ridaura VK**, **Faith JJ**, **Rey FE**, **Knight R**, **Gordon JI**. 2009. The effect of diet on the human gut microbiome: a metagenomic analysis in humanized gnotobiotic mice. Science Translational

621 Medicine **1**:6ra14–6ra14.

622 57. **David LA**, **Maurice CF**, **Carmody RN**, **Gootenberg DB**, **Button JE**, **Wolfe BE**, **Ling AV**, **Devlin AS**,
623 **Varma Y**, **Fischbach MA**, **Biddinger SB**, **Dutton RJ**, **Turnbaugh PJ**. 2014. Diet rapidly and reproducibly
624 alters the human gut microbiome. Nature **505**:559–563.

625 58. **Jeong H**, **Tombor B**, **Albert R**, **Oltvai ZN**, **Barabási AL**. 2000. The large-scale organization of metabolic
626 networks. Nature **407**:651–654.

627 59. **Grice EA**, **Kong HH**, **Conlan S**, **Deming CB**, **Davis J**, **Young AC**, **NISC Comparative Sequencing**
628 **Program**, **Bouffard GG**, **Blakesley RW**, **Murray PR**, **Green ED**, **Turner ML**, **Segre JA**. 2009. Topographical
629 and Temporal Diversity of the Human Skin Microbiome. Science **324**:1190–1192.

630 60. **Minot S**, **Bryson A**, **Chehoud C**, **Wu GD**, **Lewis JD**, **Bushman FD**. 2013. Rapid evolution of the
631 human gut virome. Proceedings of the National Academy of Sciences of the United States of America
632 **110**:12450–12455.

633 61. **Schloss PD**, **Handelsman J**. 2005. Introducing DOTUR, a computer program for defining operational
634 taxonomic units and estimating species richness. Applied and Environmental Microbiology **71**:1501–1506.

635 62. **Yilmaz S**, **Allgaier M**, **Hugenholtz P**. 2010. Multiple displacement amplification compromises
636 quantitative analysis of metagenomes. Nature Methods **7**:943–944.

637 63. **Kim KH**, **Chang HW**, **Nam YD**, **Roh SW**. 2008. Amplification of uncultured single-stranded DNA viruses
638 from rice paddy soil. Applied and ….

639 64. **Kim K-H**, **Bae J-W**. 2011. Amplification methods bias metagenomic libraries of uncultured
640 single-stranded and double-stranded DNA viruses. Applied and Environmental Microbiology **77**:7663–7668.

641 65. **Minot S**, **Wu GD**, **Lewis JD**, **Bushman FD**. 2012. Conservation of gene cassettes among diverse viruses
642 of the human gut. PLOS ONE **7**:e42342.

643 66. **Deng L**, **Ignacio-Espinoza JC**, **Gregory AC**, **Poulos BT**, **Weitz JS**, **Hugenholtz P**, **Sullivan MB**.
644 2014. Viral tagging reveals discrete populations in Synechococcus viral genome sequence space. Nature

513:242–245.

67. **Brum JR**, **Ignacio-Espinoza JC**, **Roux S**, **Doulcier G**, **Acinas SG**, **Alberti A**, **Chaffron S**, **Cruaud C**, **Vargas C de**, **Gasol JM**, **Gorsky G**, **Gregory AC**, **Guidi L**, **Hingamp P**, **Iudicone D**, **Not F**, **Ogata H**, **Pesant S**, **Poulos BT**, **Schwenck SM**, **Speich S**, **Dimier C**, **Kandels-Lewis S**, **Picheral M**, **Searson S**, **Tara Oceans Coordinators**, **Bork P**, **Bowler C**, **Sunagawa S**, **Wincker P**, **Karsenti E**, **Sullivan MB**. 2015. Ocean plankton. Patterns and ecological drivers of ocean viral communities. Science **348**:1261498–1261498.

68. **Malki K**, **Kula A**, **Bruder K**, **Sible E**, **Hatzopoulos T**, **Steidel S**, **Watkins SC**, **Putonti C**. 2015. Bacteriophages isolated from Lake Michigan demonstrate broad host-range across several bacterial phyla. Virology Journal **12**:164.

69. **Polz MF**, **Hunt DE**, **Preheim SP**, **Weinreich DM**. 2006. Patterns and mechanisms of genetic and phenotypic differentiation in marine microbes. Philosophical Transactions of the Royal Society B: Biological Sciences **361**:2009–2021.

70. **Gregory AC**, **Solonenko SA**, **Ignacio-Espinoza JC**, **LaButti K**, **Copeland A**, **Sudek S**, **Maitland A**, **Chittick L**, **Dos Santos F**, **Weitz JS**, **Worden AZ**, **Woyke T**, **Sullivan MB**. 2016. Genomic differentiation among wild cyanophages despite widespread horizontal gene transfer. BMC Genomics **17**:930.

71. **Paez-Espino D**, **Eloe-Fadrosh EA**, **Pavlopoulos GA**, **Thomas AD**, **Huntemann M**, **Mikhailova N**, **Rubin E**, **Ivanova NN**, **Kyrpides NC**. 2016. Uncovering Earth's virome. Nature.

72. **Grice EA**, **Segre JA**. 2011. The skin microbiome. Nature Reviews Microbiology **9**:244–253.

73. **Round JL**, **Mazmanian SK**. 2009. The gut microbiota shapes intestinal immune responses during health and disease. Nature reviews Immunology **9**:313–323.

74. **Hannon GJ**. FASTX-Toolkit GNU Affero General Public License.

75. **Li D**, **Luo R**, **Liu C-M**, **Leung C-M**, **Ting H-F**, **Sadakane K**, **Yamashita H**, **Lam T-W**. 2016. MEGAHIT v1.0: A fast and scalable metagenome assembler driven by advanced methodologies and community practices.

668 METHODS **102**:3–11.

669 76. **Langmead B**, **Salzberg SL**. 2012. Fast gapped-read alignment with Bowtie 2. Nature Methods
670 **9**:357–359.

671 77. **Alneberg J**, **Bjarnason BS aacute ri**, **Bruijn I de**, **Schirmer M**, **Quick J**, **Ijaz UZ**, **Lahti L**, **Loman**
672 **NJ**, **Andersson AF**, **Quince C**. 2014. Binning metagenomic contigs by coverage and composition. Nature
673 Methods 1–7.

674 78. **Hyatt D**, **LoCascio PF**, **Hauser LJ**, **Uberbacher EC**. 2012. Gene and translation initiation site prediction
675 in metagenomic sequences. Bioinformatics **28**:2223–2230.

676 79. **Kuhn M**. caret: Classification and Regression Training.

677 80. **Edgar RC**. 2007. PILER-CR: fast and accurate identification of CRISPR repeats. BMC Bioinformatics
678 **8**:18.

679 81. **Camacho C**, **Coulouris G**, **Avagyan V**, **Ma N**, **Papadopoulos J**, **Bealer K**, **Madden TL**. 2009. BLAST+:
680 architecture and applications. BMC Bioinformatics **10**:1.

681 82. **Buchfink B**, **Xie C**, **Huson DH**. 2015. Fast and sensitive protein alignment using DIAMOND. Nature
682 Methods **12**:59–60.

683 83. Neo4j.

684 84. **Csardi G**, **Nepusz T**. The igraph software package for complex network research.